LBL-14840
Preprint

Lawrence Berkeley Laboratory
UNIVERSITY OF CALIFORNIA

Materials & Molecular
Research Division

Submitted to Physical Review B

SURFACE-ENHANCED SECOND-HARMONIC GENERATION AND RAMAN SCATTERING

C.K. Chen, T.F. Heinz, D. Ricard, and Y.R. Shen

August 1982

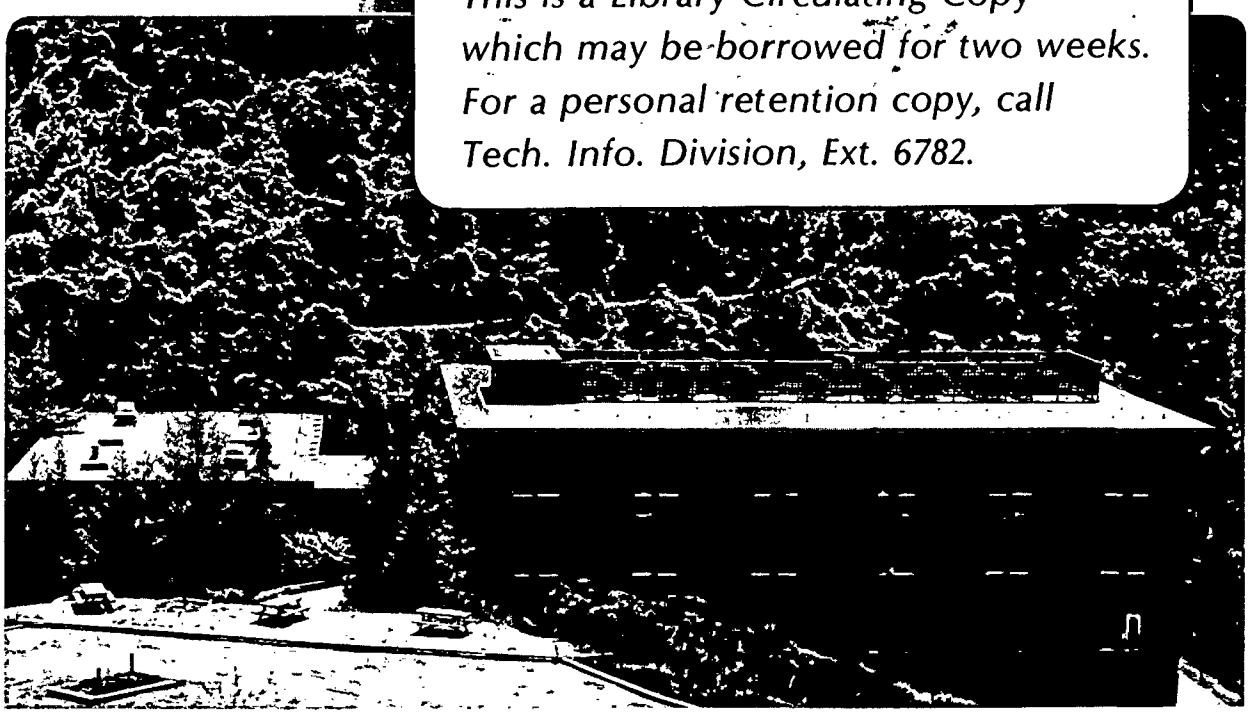

Prepared for the U.S. Department of Energy under Contract DE-AC03-76SF00098

DISCLAIMER

Submitted to The Physical Review B LBL-14840
PACS 42.65. Cq, 68.45.-v, 07.60.-j; 82.65.-i.

SURFACE-ENHANCED SECOND-HARMONIC GENERATION AND RAMAN SCATTERING*

C. K. Chen,[a] T. F. Heinz, D. Ricard,[b] and Y. R. Shen[c]

Department of Physics
University of California
Berkeley, California 94720

and

Materials and Molecular Research Division
Lawrence Berkeley Laboratory
Berkeley, California 94720

ABSTRACT

Emission from a variety of surface optical processes is significantly increased at interfaces with roughened noble metals. A general formalism, applicable to any optical process, is used to predict the enhancement in the radiated power for second-harmonic generation and Raman scattering from an electrochemically reformed silver surface. Experimental results for these enhancements at different wavelengths are reported. The intensity of the second-harmonic radiation can be understood strictly in terms of the strong macroscopic electric fields produced at the roughened surface by resonant structures. For Raman scattering, part of the enhancement also arises from microscopic local-field effects and the direct chemical interaction of the adsorbate and substrate. The surface-enhanced second-harmonic and Raman signals are studied as the silver sample undergoes oxidation and reduction in an electrolyte containing cyanide ions. The behavior of these two easily measurable probes is described and correlated with the system's surface chemistry.

*This work was supported by the Director, Office of Energy Research, Office of Basic Energy Sciences, Materials Sciences Division of the U.S. Department of Energy under Contract Number DE-AC03-76SF00098.

I. Introduction

Raman scattering by pyridine adsorbed on electrochemically reformed silver was discovered a few years ago to exhibit an effective cross-section increased above that of the free molecule by several orders of magnitude.[1] This phenomenon of surface-enhanced Raman scattering (SERS) has attracted and continues to attract considerable attention.[2] An appreciable enhancement has been manifested by a wide range of molecular adsorbates on surfaces of various metals at solid/liquid,[1,2] solid/vacuum,[3-6] and even at solid/solid[7,8] interfaces. As researchers have recognized the common features of surface roughness [3-17] and small optical absorption [18] of substrates exhibiting prominent enhancement, it has come to be accepted that the macroscopic electrodynamics of the surface plays a significant role in SERS: the presence of the roughened metal can produce a local field strength at the interface which greatly exceeds that of the applied field.[19-25] This mechanism of local-field enhancement should affect all surface optical processes. In fact, significant surface enhancements have been reported for hyper-Raman scattering,[26] for one- and two-photon absorption and luminescence,[27-29] and for second-harmonic generation (SHG) by bare metals[30,31] and molecular adsorbates.[32,33] The SHG process is of particular interest since the signal can originate from the metal alone. Furthermore, the fact that it is forbidden in the bulk of a centrosymmetric medium endows SHG with an intrinsic surface sensitivity.

The theory of local-field enhancements has been developed by a number of authors to treat the specific surface optical process under consideration.[14-32] In this paper we elaborate the theory in a more general fashion. By extending the notion of a correction to the molecular polariz-

ability from microscopic local fields to macroscopic ones, we can describe directly the amplification of the incident and radiated fields induced by the presence of the surface. The surface enhancement of any particular process can then be readily calculated. We present this formalism and some model calculations in Sec. II.

On the experimental side, while both surface-enhanced Raman scattering and SHG have been observed, they have not been simultaneously measured and correlated with the different phases of oxidation-reduction cycles in an electrochemical cell. The Raman and second-harmonic signals from a silver electrode were monitored while cycling in pure electrolytes (K_2SO_4 or KCℓ) and while cycling with cyanide ions also present. In the latter case, a rich surface chemistry resulted. The rather different responses of the two optical probes could be interpreted with the aid of voltammograms indicating the onset of various reactions. The experimental procedure and the results of the combined second-harmonic and Raman scattering measurements are found in Secs. III and IV. In the latter part of Sec. IV, the theory of sec. II is applied to a simple model of a roughened surface consisting of small hemispheroids on a conducting plane. Predictions are made of the macroscopic local-field enhancements for SHG and Raman scattering. Experimental values for both processes with identical excitation of a given sample can then be compared. For the chosen pump radiation, the second-harmonic nonlinearity proves to be dominated by that of the silver itself. For this case, the macroscopic local-field corrections should completely account for the surface enhancement. From the experimental Raman scattering power, we can then estimate the residual enhancement of the Raman cross-section associated with microscopic local fields

and the direct molecule-metal interaction. In the closing section of the paper, we draw some conclusions and, as a further example of the local-field theory, calculate the surface enhancement for coherent anti-Stokes Raman scattering by an adsorbate.

II. Theory of Local-Field Enhancement

A. General Formalism

The mechanisms leading to the enhancement of various optical processes at surfaces can be broken down into two broad categories: those involving a change in the nature of the adsorbate by means of a direct interaction with the substrate and those involving only a modification of the local electric and magnetic fields caused by the presence of the substate. The former group of chemical effects has been invoked in various explanations of SERS[2] and notably in understanding SERS by normally Raman-inactive modes of adsorbates[34,35] and SHG by centrosymmetric adsorbates.[33] The electromagnetic effects of local-field enhancements are now believed to be the main contributor to SERS of Raman-active modes of adsorbates, and they are the only contributor to the enhancement of SHG from bare metal surfaces.[30,31] We shall present here a general formalism for treating this local-field enhancement.

Let us first consider an isolated molecule in space surrounded by radiation fields $E(\omega_1)$, $E(\omega_2)$, ..., $E(\omega_n)$ with angular frequencies ω_1, ω_2, ..., ω_n. An n-th order nonlinear dipole $p^{(n)}(\omega = \omega_1 + \omega_2 + \ldots + \omega_n)$ can then be induced in the molecule through the nonlinear polarizability $\overleftrightarrow{\alpha}^{(n)}(\omega = \omega_1 + \omega_2 + \ldots + \omega_n)$:

$$\vec{p}^{(n)}(\omega) = \overleftrightarrow{\alpha}^{(n)} : \vec{E}(\omega_1) \ \ldots \ \vec{E}(\omega_n). \tag{1}$$

If, however, the molecule is sitting near a surface and if it is also surrounded by other molecules, it will experience a local field $\vec{E}_{loc}(\omega_i)$ different from the incoming field $\vec{E}(\omega_i)$ of Eq. (1). In this case, the induced dipole will be given by

$$\vec{p}^{(n)}(\omega) = \overleftrightarrow{\alpha}^{(n)} : \vec{E}_{loc}(\omega_1) \ \ldots \ \vec{E}_{loc}(\omega_n). \tag{2}$$

These local fields can be attributed to two distinct effects: the change in the microscopic fields and the change in the average or macroscopic fields. The local variation in the microscopic fields arising from the induced dipole-dipole interaction is the usual Lorentz correction discussed in the literature.[36] In a homogeneous liquid, for example, it yields the familiar Lorenz - Lorentz relation of $\ell(\omega_i) = [\varepsilon(\omega_i) + 2]/3$. The microscopic local-field correction for molecules adsorbed on a surface has recently been discussed by Bagchi et al.[37] and also in connection with image-dipole models for SERS.[2,38-40] The change in the macroscopic field at the surface compared with the applied field is just what we expect from reflection and refraction of the incident field. We can call this a macroscopic local field, which, in principle, is obtained from the solution of the wave equation with the appropriate boundary conditions at the surface. The macroscopic local-field correction factor $\overleftrightarrow{L}(\omega)$ is then the ratio of the macroscopic local field to the incident field. As we shall see, this factor can be substantial for metals with resonant structures on the surface. Taking account of both the macroscopic and microscopic

corrections, we can write for the local electric field

$$\vec{E}_{loc}(\omega_i) = \overleftrightarrow{\ell}(\omega_i)\overleftrightarrow{L}(\omega_i):\vec{E}(\omega_i). \tag{3}$$

The nonlinear dipole $\vec{p}^{(n)}(\omega)$ induced by the local fields now radiates. Since the neighboring dipoles also respond to this excitation at frequency ω, the radiation appears as if $\vec{p}^{(n)}(\omega)$ were enhanced by an additional local-field correction factor $\overleftrightarrow{\ell}(\omega)$ (Ref. 41). Similarly, through the interaction of $\vec{p}^{(n)}(\omega)$ with the surface, the macroscopic field at ω is also enhanced by a further factor of $\overleftrightarrow{L}(\omega)$. Thus, the radiated field from the nonlinear dipole at the surface in an ambient dielectric with constant ε is [42]

$$\vec{E}^{dip}_{out}(\omega) = e^{ikr}(k^2/\varepsilon r)[(\hat{n} \times \vec{p}_{eff}(\omega)) \times \hat{n}], \tag{4a}$$

where

$$\vec{p}^{(n)}_{eff}(\omega) = \overleftrightarrow{\alpha}^{(n)}:\overleftrightarrow{\ell}(\omega)\overleftrightarrow{L}(\omega)\overleftrightarrow{\ell}(\omega_1)\overleftrightarrow{L}(\omega_1) \ \ldots \ \overleftrightarrow{\ell}(\omega_n)\overleftrightarrow{L}(\omega_n)\vec{E}(\omega_1) \ \ldots \ \vec{E}(\omega_n). \tag{4b}$$

Here $k = \sqrt{\varepsilon}\ (\omega/c)$ and $\hat{n}$ is the direction of propagation of the outgoing field. The total radiated field from a collection of dipoles is, of course, obtained by summing over the individual contributions. If the process is coherent, as for SHG, the resulting radiated field can be expressed as

$$\vec{E}_{out}(\omega) = \int_S d^2x_s N(\vec{x}_s) e^{ikr}(k^2/\varepsilon r)[(\hat{n} \times \vec{p}^{(2)}_{eff}(\omega,\vec{x}_s)) \times \hat{n}], \tag{5a}$$

with the integration extended over the surface covered by the nonlinear dipoles of density $N(\vec{x}_s)$. The total output power in a solid angle Ω from the radiating dipoles is found in the usual manner from[43]

$$\mathscr{P}_{coh}(\omega) = (c\sqrt{\varepsilon}/2\pi) \int_{\Omega} r^2 d\Omega |\vec{E}_{out}(\omega)|^2. \tag{5b}$$

If, however, the nonlinear dipoles radiate incoherently, as in the case of Raman scattering, then the output is given by

$$\mathscr{P}_{inc}(\omega) = (c\sqrt{\varepsilon}/2\pi) \int_{\Omega} r^2 d\Omega \int_{S} d^2x_s N(\vec{x}_s) |\vec{E}^{dip}_{out}(\omega, \vec{x}_s)|^2. \tag{6}$$

Thus, for a specified surface with known local-field correction factors, we should be able to calculate the output power. The local-field enhancement is defined as the ratio of the radiated power in the case of interest to that of a reference. For example, for SERS, the reference can be chosen as the molecules in the gas or liquid phase; for surface-enhanced SHG by a metal, the bare, flat surface can be taken as the standard. As discussed below, the electrolytically roughened silver surface used in the current set of experiments exhibited an enhancement of the Raman scattering of $\sim 10^6$ for visible radiation, with a corresponding second-harmonic enhancement of $\sim 10^2$ for a visible pump and $\sim 10^4$ for near-infrared excitation.

In the following, we shall discuss a few special geometries of the metal-dielectric interface. Microscopic local-field corrections will not be taken into account. As a rough estimate of this effect, we can apply the theory of Bagchi et al.[37] for isotropic molecules in a square lattice

of spacing 5 Å located 2.5 Å above a conducting plane. In this case, with a linear polarizability of $\alpha^{(1)} = 10$ Å^3, the microscopic local-field correction factors for electric fields parallel and perpendicular to the surface are found to be $\ell_{\parallel} = 1.6$ and $\ell_{\perp} = 0.6$. On the other hand, according to the Lorenz-Lorentz formula for a homogeneous liquid, the local-field correction factor for water ($\varepsilon = 1.77$) is $\ell = 1.3$.

B. Special Cases

We consider here three different geometries for the interface between a metal substrate, characterized by a (local) dielectric constant $\varepsilon_m(\omega)$, and the ambient dielectric medium with a real, dispersionless dielectric constant ε. A thin intermediate region of dielectric constant $\varepsilon'(\omega)$ is included to describe an adsorbed molecular layer. We first treat the simple planar boundary. Then, as an approximation of a roughened surface, we analyze the case of a small metal hemisphere lying on an infinite plane, which, for simplicity, is taken to be a perfect conductor. These hemispherical protrusions exhibit resonant response to an applied field when $\mathrm{Re}(\varepsilon_m(\omega) + 2\varepsilon) = 0$. Finally, as a more refined model of an electrochemically roughened metal surface, we extend our calculations to the case of a hemispheroidal boss on a conducting plane.

1. Planar Interface

In this instance, the Fresnel coefficients for the reflection and refraction of waves at a planar boundary give the relation between the incoming macroscopic fields and the macroscopic fields present at the interface, i.e., the macroscopic local-field factors. The local-field tensor $\overleftrightarrow{L}$ becomes diagonal when expressed with respect to the surface normal and

directions parallel to the surface lying in and normal to the plane of incidence of the wave:

$$L_{\perp} = (\varepsilon/\varepsilon')2\sqrt{\varepsilon_m}\cos\theta/(\sqrt{\varepsilon_m}\cos\theta + \sqrt{\varepsilon}\cos\theta_m)$$

$$L_{\parallel}^{p} = 2\sqrt{\varepsilon}\cos\theta_m/(\sqrt{\varepsilon_m}\cos\theta + \sqrt{\varepsilon}\cos\theta_m)$$

$$L_{\parallel}^{s} = 2\sqrt{\varepsilon}\cos\theta_m/(\sqrt{\varepsilon}\cos\theta + \sqrt{\varepsilon_m}\cos\theta_m). \qquad (7)$$

The superscripts p and s refer, respectively, to the components parallel and perpendicular to the plane of incidence. θ denotes the angle of incidence of the light and θ_m is the angle of refraction. The expressions above apply to the fields in the dielectric layer of constant ε' just above the metal, but they are also valid for the fields just inside the metal if $\varepsilon' = \varepsilon_m$.

With the given local-field factor $\overleftrightarrow{L}$, we can calculate the radiated power by means of Eq. (4), in conjunction with Eq. (5) for a coherent process and with Eq. (6) for an incoherent one. For Raman scattering by a layer of aligned molecules with surface density N and Raman polarizability $\overleftrightarrow{\alpha}^{R}$, we find a total power

$$\mathcal{P}_R(\omega_s) = (c\sqrt{\varepsilon}/2\pi)(\omega_s/c)^4 N\mathcal{A}\int_{\Omega} d\Omega\,|\hat{n}\times\overleftrightarrow{\alpha}^{R}:\overleftrightarrow{L}(\omega_s)\overleftrightarrow{L}(\omega)\vec{E}(\omega)|^2. \qquad (8)$$

Here the pump beam of frequency ω illuminates an area $\mathcal{A}$ of the interface; $\hat{n}$ gives the direction of the outgoing radiation at the Stokes-shifted frequency ω_s; and the tensor $\overleftrightarrow{L}$ is specified by Eq. (7). In the limit of

$|\varepsilon_m| \gg \varepsilon = \varepsilon'$, the macroscopic local-field factors simplify to $L_{\parallel}^{p} = L_{\parallel}^{s} = 0$ and $L_{\perp} = 2$. In this case, the total radiated power under pumping by a p-polarized beam with field strength $E(\omega)$ incident at angle θ is

$$\mathcal{P}_R(\omega_s) = (32c\sqrt{\varepsilon}/3)(\omega_s/c)^4 N\mathcal{A}|\alpha_{\perp\perp}^R|^2 E^2(\omega)\sin^2\theta. \qquad (9)$$

With excitation at grazing incidence, this radiated power exceeds by a factor of 8 that emitted by an equal number of isolated isotropically polarizable Raman scatterers in the bulk dielectric medium.

In the case of SHG, we are dealing with a coherent process and, consequently, a uniform adsorbed layer with a nonlinear response will give rise to a collimated beam of second-harmonic radiation in the reflected direction. Equations (5) and (6) yield for the power in this beam at the harmonic frequency

$$\mathcal{P}_{SH}(2\omega) = (2\pi c/\sqrt{\varepsilon})(2\omega/c)^2 N^2\mathcal{A}|\hat{n} \times \overleftrightarrow{\alpha}^{(2)} : \overleftrightarrow{L}(2\omega)\overleftrightarrow{L}(\omega)\overleftrightarrow{L}(\omega)\vec{E}(\omega)\vec{E}(\omega)|^2 \sec\theta. \qquad (10)$$

$\overleftrightarrow{\alpha}^{(2)}$ represents the second-order nonlinear polarizability of the adsorbed species, of which an area $\mathcal{A}$ ($\gg k^{-2}$) is exposed to radiation at the fundamental frequency ω. The same result (with the proper $L_{\perp}$) applies for SHG by the surface layer of the metal itself. More specifically, let us write for later use the expression in the case of p-polarized excitation of a nonlinearity having only a significant $\|\perp\|$-component:

$$\mathcal{P}_{SH}(2\omega) = (2\pi c/\sqrt{\varepsilon})(2\omega/c)^2 N^2\mathcal{A}|\alpha_{\|\perp\|}^{(2)} L_{\|}^{p}(2\omega) L_{\perp}(\omega) L_{\|}^{p}(\omega)|^2 E^4(\omega)\cos^3\theta \sin^2\theta. \qquad (11)$$

2. Hemispherical Boss

In the interest of simplicity, the base plane on which the metal hemisphere rests is presumed to be perfectly conducting; the hemisphere itself is taken to be much smaller than a wavelength of light so that retardation effects need not be considered and the macroscopic local fields can be determined by electrostatics. The presence of the conducting plane causes the component of the incident electric field normal to the surface to be doubled, while cancelling the tangential part. Then by solving the elementary boundary-value problem, we can find the relation between the macroscopic local field at a point on the hemisphere and the field present above the conducting plane, namely,

$$L_{\perp} = (\varepsilon_m/\varepsilon')3\varepsilon/(\varepsilon_m + 2\varepsilon)$$

$$L_{\parallel} = 3\varepsilon/(\varepsilon_m + 2\varepsilon). \qquad (12)$$

The tensor $\overleftrightarrow{L}$ assumes this diagonal form for any given point on the hemisphere when resolved into components perpendicular to and lying in the local tangent plane at the hemispherical surface. With the aid of these local-field factors, we can now immediately compute the scattered power for the Raman and SHG processes.

The total power of Raman scattered light is specified by Eqs. (4) and (6). For a p-polarized pump beam of frequency ω making an angle θ with the conducting plane, an adsorbate-covered hemispherical boss of radius a produces a total output at the Raman-shifted frequency ω_s of

$$\mathscr{P}_R(\omega_s) = (64\pi c\sqrt{\varepsilon}/15)(\omega_s/c)^4 N a^2 |\alpha^R_{\perp\perp} L_\perp(\omega_s) L_\perp(\omega)|^2 E^2(\omega) \sin^2\theta. \qquad (13)$$

This expression was derived assuming that only the $\perp\perp$-component of the Raman polarizability was important, as is the case if $|L_\perp| = |\varepsilon_m/\varepsilon'||L_\parallel| \gg |L_\parallel|$, i.e., whenever $|\varepsilon_m/\varepsilon'| \gg 1$. Comparing this result to that for Raman scattering from isolated, isotropically polarizable molecules in the bulk dielectric medium, we obtain the surface enhancement attributable to macroscopic local-field effects. Forming the ratio of total scattered power per molecule, we deduce for this quantity

$$\eta_R = (8/5)|L_\perp(\omega_s) L_\perp(\omega)|^2 \sin^2\theta. \qquad (14)$$

Second-harmonic radiation emitted by the adsorbate-covered hemisphere is angularly diffuse. If only the $\parallel\perp\parallel$-component of the quadratic polarizability is appreciable, the total second-harmonic power radiated in all directions for excitation by a p-polarized pump is given by Eqs. (4) and (5) as

$$\mathscr{P}_{SH}(2\omega) = (32\pi^2 c\sqrt{\varepsilon}/3)(2\omega/c)^4 N^2 a^4 |\alpha^{(2)}_{\parallel\perp\parallel} L_\parallel(2\omega) L_\perp(\omega) L_\parallel(\omega)|^2 E^4(\omega) \sin^4\theta. \qquad (15)$$

Dividing this radiated power by that for an equal area of an equivalent flat surface also excited by a p-polarized pump incident at angle θ, we arrive at the surface-enhancement factor

$$\eta_{SH} = (32/3)(ka)^2 \sin^2\theta \sec^3\theta \frac{|L_\parallel(2\omega) L_\perp(\omega) L_\parallel(\omega)|^2_{\text{sphere}}}{|L^p_\parallel(2\omega) L_\perp(\omega) L^p_\parallel(\omega)|^2_{\text{plane}}}. \qquad (16)$$

Here $k = \sqrt{\varepsilon}\,\omega/c$ and the local-field factors in the numerator and denominator are those of Eq. (12) and of Eq. (7), respectively.

Neglecting the geometric factors resulting from averaging and normalization, we find from Eq. (14) that the surface enhancement for Raman scattering has the form $\eta_R \sim |L(\omega_s)L(\omega)|^2$; for SHG, Eq. (16) implies that $\eta_{SH} \sim (ka)^2|L(2\omega)L^2(\omega)|^2$. The former expression is just what we expect for incoherent scattering by the Raman process, the enhancement being proportional to the cross-section σ_R, which, in turn, varies as $|\alpha^R|^2$. In the case of SHG, we must compare the signal from the hemispherical surface to that from a plane. In the plane, an area $\sim \lambda^2 = (2\pi/k)^2$ can radiate in phase for this coherent process, but for the hemisphere of radius a, only its surface area $2\pi a^2$ can do so. For this reason, in addition to the obvious terms for a signal proportional to $|\alpha^{(2)}(2\omega = \omega + \omega)|^2$, an extra factor of $(ka)^2$ is introduced into the formula for η_{SH}. Now inspection of Eq. (12) reveals that when the denominator $\varepsilon_m + 2\varepsilon$ approaches zero, we obtain a large value for the local-field factors, and, hence, for the Raman and second-harmonic surface enhancements as well. Since this denominator must always have a positive imaginary part, the optimal enhancement should occur for $\mathrm{Re}(\varepsilon_m + 2\varepsilon) = 0$, corresponding to the excitation of a local surface plasmon. Noble metals, which typically have dielectric constants with negative real and small imaginary parts for infrared and visible light, can exhibit considerable surface enhancements through this mechanism.

3. Hemispheroidal Boss

Here we take up the generalization of the previous geometry to the case of a hemispheroidal boss with a semimajor axis of length a normal to

the conducting plane and a semiminor axis of length b. The assumption of $ka \ll 1$ is maintained to allow an electrostatic analysis. The macroscopic local fields on the protrusion are related to the field above the conducting plane in the same way as the fields on a full spheroid are related to a constant applied field directed along the principal axis. The solution to this classic problem[44] can be expressed succinctly with respect to the local surface normal and tangential directions. The resulting local-field factors are

$$L_{\perp} = (\varepsilon_m/\varepsilon')\varepsilon/[\varepsilon + (\varepsilon_m - \varepsilon)A]$$

$$L_{\parallel} = \varepsilon/[\varepsilon + (\varepsilon_m - \varepsilon)A]. \tag{17}$$

The depolarization factor A takes on the value of 1/3 for a sphere and approaches 0 for a very slender prolate spheroid.[45] For the geometry under consideration the local surface plasmon resonance now occurs for $\mathrm{Re}[\varepsilon + (\varepsilon_m - \varepsilon)A] = 0$. The local-field enhancement can be particularly large for highly elongated spheroids, since in the limit of $A \to 0$, $\mathrm{Im}[\varepsilon + (\varepsilon_m - \varepsilon)A]$ will decrease, causing the resonant enhancement to grow. This behavior can be termed a lightning rod effect.[23,24]

From Eqs. (4) and (6), we can obtain the Raman scattered power from the hemispheroidal protrusion covered uniformly by an adsorbate. For a p-polarized pump,

$$\mathscr{P}_R(\omega_s) = (64\pi c\sqrt{\varepsilon}/3)(\omega_s/c)^4(b/a)^4 N a^2 |\alpha^R_{\perp\perp} L_{\perp}(\omega_s) L_{\perp}(\omega)|^2 E^2(\omega)\sin^2\theta. \tag{18}$$

As before, this formula is valid if only the $\perp\perp$-component of the Raman

polarizability is important, which holds whenever $|\varepsilon_m/\varepsilon'| \gg 1$. This and subsequent expressions are also simplified by taking the protrusion to be highly elongated ($a/b \gg 1$). The macroscopic local-field enhancement in the radiated power is given by the ratio of Eq. (18) to the power radiated by an equal number $N\mathscr{A} \approx N\pi^2 ab/2$ of isolated molecules in the bulk dielectric medium:

$$\eta_R = (32/\pi)(b/a)^3 |L_\perp(\omega_s)L_\perp(\omega)|^2 \sin^2\theta. \tag{19}$$

For SHG by a uniform layer of an adsorbate with only a $\|\perp\|$-component of the nonlinearity, we deduce, according to Eqs. (4) and (5), a radiated harmonic power under p-polarized excitation of

$$\mathscr{P}_{SH}(2\omega) = (2^7\pi^2 c\sqrt{\varepsilon}/3)(2\omega/c)^4 (b/a)^4 N^2 a^4 |\alpha^{(2)}_{\|\perp\|} L_\|(2\omega)L_\perp(\omega)L_\|(\omega)|^2 E^4(\omega)\sin^4\theta. \tag{20}$$

The enhancement with respect to SHG by an equal area of the adsorbate-covered metal plane is then found to be

$$\eta_{SH} = (2^9/3\pi)(b/a)^3 (ka)^2 \sin^2\theta \sec^3\theta \frac{|L_\|(2\omega)L_\perp(\omega)L_\|(\omega)|^2_{spheroid}}{|L^p_\|(2\omega)L_\perp(\omega)L^p_\|(\omega)|^2_{plane}}. \tag{21}$$

The local-field factors in this expression are those of Eqs. (7) and (17); the factor of $(ka)^2$ arises from the coherence of the SHG process, as discussed above for the hemispherical boss. In Sec. IV, we shall see how the large observed enhancements of SHG and Raman scattering are predicted by resonant excitation of these surface features.

C. Second-Harmonic Generation from Metal Surfaces

In order to apply our formalism of local-field enhancements to the problem of SHG by metal surfaces, we must determine the form of the relevant nonlinear source polarization. Within the interior of a centrosymmetric medium the electric-dipole contribution to the second-order nonlinearity vanishes. Then for a medium that is also isotropic (such as the polycrystalline silver samples of the experiment described in the following sections), the most general form of the nonlinearity from the magnetic-dipole and electric-quadrupole terms can be expressed as[46]

$$\vec{P}^{(2)}(2\omega) = \beta[\nabla \cdot \vec{E}(\omega)]\vec{E}(\omega) + (\delta - \beta)[\vec{E}(\omega) \cdot \nabla]\vec{E}(\omega) + \gamma(i2\omega/c)\vec{E}(\omega) \times \vec{H}(\omega), \tag{22}$$

with parameter β, γ, and δ being characteristic of the material under study. Inside a homogeneous medium, the first term must vanish, as must the second when $\vec{E}(\omega)$ represents a plane wave. At the surface of the metal, however, the discontinuity in the normal component of $\vec{E}(\omega)$ causes both of these terms to produce a singular layer of polarization. The third term in the expression for $\vec{P}^{(2)}(2\omega)$ only gives a contribution in the bulk. Various model calculations have been carried out to predict the values of these coefficients, yet for visible light the problem remains a difficult one, since one must generally consider both the detailed nature of the surface and the effect of interband transitions.[46-50]

For the first few atomic layers of a metal (or for adsorbates), the inversion symmetry of the bulk metal is clearly broken. Consequently, an electric-dipole contribution to the second-order nonlinearity is expected from the surface. We can express such a term as a nonlinear susceptibility $\overleftrightarrow{\chi}_s^{(2)}$

localized at the surface. Symmetry arguments imply that this tensor has only three independent coefficients for SHG: $\chi^{(2)}_{s\parallel\perp\parallel} = \chi^{(2)}_{s\parallel\parallel\perp}$, $\chi^{(2)}_{s\perp\parallel\parallel}$, and $\chi^{(2)}_{s\perp\perp\perp}$. While the physical origin of this dipole contribution is certainly different from that of the magnetic-dipole and electric-quadrupole terms, it so happens that the inclusion of the electric-dipole contribution does not alter the form of either the polarization or angular dependences of the second-harmonic signal.[51] In fact, we are not aware of any experiment that has explicitly resolved these two mechanisms. For our present purpose, we can just consider a nonlinear polarization of the form of Eq. (22) with parameters β, γ, and δ modified to include the contribution of the three independent components of $\overleftrightarrow{\chi}^{(2)}_s$.

We have analyzed the experimental dependence of the second-harmonic reflection on the angle of incidence of a p-polarized pump beam reported by Sonnenberg and Heffner[52] and Bloembergen et al.[46] for a flat silver sample. Using the correct solution of Maxwell's equations for a nonlinearity of the form of Eq. (22) (see erratum for Ref. 46), we have found that δ is negligible for excitation at the ruby laser wavelength of 0.694 μm. As for the relative importance of the β and γ terms, Wang and Duminski[53] have deduced from their measurements also made with a ruby laser that $|\gamma/\beta| = 3.7$. For p-polarized excitation with $\theta \sim 45°$, we then find that the γ term actually contributes somewhat less to the radiated signal than does the β term. Given the variation of experimental results in the literature and the crudeness of our models for the roughened surface, we shall not attempt to compare these terms more closely, but shall simply neglect γ. It should be noted that in the case of resonant excitation of small surface features of the metal, this approximation is very accurate if γ actually represents

a bulk (and not an effective surface) polarization. In this case, the magnetic field in the source polarization term $\gamma(2i\omega/c)\vec{E}(\omega) \times \vec{H}(\omega)$ does not show the full enhancement.

Thus, for our discussion of surface enhancement,[54] we shall consider the nonlinearity of the metal to be described by[55]

$$\vec{P}^{(2)}(2\omega) = \beta\{[\nabla \cdot \vec{E}(\omega)]\vec{E}(\omega) - [\vec{E}(\omega) \cdot \nabla]\vec{E}(\omega)\}. \qquad (23)$$

For either excitation of a flat sample by a single plane wave or for any excitation of a structure small compared to a wavelength, this term is only significant at the surface itself where $\vec{E}(\omega)$ changes abruptly. Integrating $\vec{P}^{(2)}(2\omega)$ across the interface,[46] we find that we can also describe this nonlinearity by a surface dipole term with susceptibility $N\alpha^{(2)}_{\parallel\perp\parallel} = \beta[\varepsilon_m(\omega) - \varepsilon'(\omega)]$ lying just inside the metal or, equivalently, a polarizable sheet with $N\alpha^{(2)}_{\parallel\perp\parallel} = \beta[\varepsilon_m(\omega)/\varepsilon'(\omega) - 1]$ located in the intermediate dielectric layer ε'. In the latter case, the previously developed equations for the second-harmonic power and enhancement can be applied directly to the signal generated by the metal.

III. Experimental Arrangement

Our experimental studies were designed to compare signals from the two surface probes of Raman scattering and second-harmonic generation during an electrochemical cycle , as well as to determine the surface enhancement exhibited by these two optical processes. The Raman scattering and second-harmonic emission from a silver sample were monitored during and after various electrochemical reactions. The set-up is depicted schematic-

ally in Fig. 1. The polycrystalline silver electode was prepared by mechanical polishing, etching for several minutes in a 1:1 volume mixture of H_2O_2(30%):NH_4OH, and a thorough rinsing in distilled water. The electrochemical cell, which was equipped with a platinum wire counter electrode and a reference saturated calomel electrode (SCE), contained a 0.1M K_2SO_4 or KCℓ electrolyte in doubly distilled water. Before any measurements were made, the sample surface was roughened and cleaned by running several oxidation-reduction cycles. Each cycle provided a charge transfer of $\sim$ 100mC/cm^2, corresponding to an average removal and redeposition of some 400 atomic layers of the flat silver surface. This procedure yielded a silver sample capable of inducing an enhancement of $\sim 10^6$ for Raman scattering by adsorbed pyridine.

Optical excitation for the SHG and Raman scattering processes consisted of the 10 ns pulses of 0.683 μm radiation. These pulses, available at a repetition rate of 10 Hz, were generated by a hydrogen Raman cell pumped by the second harmonic of a Q-switched Nd:YAG laser. So as to avoid laser-induced damage or desorption at the silver surface, fluences were limited throughout these experiments to $\sim$ 1 mJ/cm^2. We verified that the effect of the laser radiation was minimal by observing the same variation of the signals during electrochemical reactions at still lower fluences. The SERS response for cw excitation by the 0.514 μm output of an argon ion laser also duplicated that obtained with the pulsed excitation. The nonlinearity for SHG by the silver substrate alone shows a marked dispersion, being much larger at a wavelength of 0.7 μm than at 1.0 μm (Ref. 46). Consequently, for our study of the second-harmonic signal during electrolytic cycling, we found it advantageous to use the 1.06 μm funda-

mental of the Q-switched Nd:YAG laser as a pump. The angularly diffused Raman and surface-enhanced second-harmonic radiation was collected with f/1 optics. The desired signals were detected with photomultipliers. For Raman scattering, the output wavelength was selected with a 3/4-meter double monochromator. A smaller monochromator together with color and interference filters proved adequate for measurements of SHG, the quadratic power dependence and spectral purity of which were checked. The Raman and second-harmonic signals were stored in a minicomputer. The computer also controlled the Ag-Pt bias and recorded the Ag-SCE potential, V_{Ag-SCE}, and the electrolytic current, I, during the oxidation-reduction cycles.

IV. Experimental Results and Discussion

A. Correlations between SHG and SERS

In this section we describe the variation of the SHG by a silver electrode during different oxidation-reduction cycles and compare the results with those of SERS. For the measurements now under discussion, both the second-harmonic and Raman signals arose primarily from the adsorbed species, as the background from the silver itself was relatively weak.

The first case to be considered is that of an oxidation-reduction cycle in a pure 0.1M K_2SO_4 electrolyte. The applied Ag-Pt voltage was ramped at a constant rate from -2.5V to +2.5V and back to -2.5V, where it was subsequently held fixed. The voltammogram for this process and the component Ag-SCE voltage and electrolytic current as functions of time are displayed in Fig. 2. During the oxidation half-cycle, the silver electrode

undergoes the reaction $Ag \rightarrow Ag^+ + e^-$. It is expected that some of the moderately soluble Ag_2SO_4 salt will form on the silver surface.[56] In the reduction half-cycle, the silver surface is reformed from the oxidized silver layer and from the Ag^+ ions in solution. It should be noted, however, that the full charge of the oxidation half-cycle is not recovered. The small second-harmonic signal [Fig. 2(b)] shows no clear increase with charge transfer during the cycle. Such a behavior can be understood if we realize that layers of an adsorbate beyond the one in direct contact with the silver substrate are not expected to be significantly ordered and, therefore, should not contribute appreciably to the SHG. The overall weakness of the second-harmonic signal in the present case is reasonable in view of the high symmetry of the Ag_2SO_4 structure.

Upon addition to the electrolyte of sufficient KCN to form a 0.01M solution, the observed behavior becomes much more complicated. The SERS of this system has already been the subject of several studies.[35,56-59] By recording the SERS spectra during the course of oxidation-reduction cycles, Benner et al.[56] have identified various phases of the process. Applying their results to our voltammogram of Fig. 3(a), we can associate the peaks labeled a, b, e, and f with the following half-reactions:

$$Ag + n(CN^-) \underset{f}{\overset{a}{\rightleftarrows}} [Ag(CN)_n]^{(n-1)-} + e^- , \quad n = 2,3,4$$

$$Ag + CN^- \underset{e}{\overset{b}{\rightleftarrows}} AgCN + e^-$$

The analysis of Benner et al. was based on resolving the different vibrational frequencies of AgCN and the silver-cyanide complexes $[Ag(CN)_n]^{(n-1)-}$.

The SERS signal for a 2110 cm^{-1} Stokes shift, corresponding to the line-center for the C-N stretch mode of $[Ag(CN)_3]^{2-}$, is indicated in our Fig. 3(b). Some silver-cyanide complexes are apparently already present on the electrode surface at the beginning of the cycle. Near point b, AgCN displaces the complexes, and the associated Raman signal starts to fall. The Raman signal from the silver-cyanide complexes grows again at the end of the cycle. The reduction of AgCN frees CN^- ions which can then form the $[Ag(CN)_n]^{(n-1)-}$ complexes, some of which eventually remain on the bare silver surface. The SERS associated with AgCN appears to be quite weak. In the studies of Benner et al., it is barely discernible near points b and e of the electrolytic cycle.

Let us now analyze the second-harmonic output for this process. In contrast to the situation for cycling in the pure K_2SO_4 electrolyte, here the presence of dissolved KCN induces a strong and abruptly changing second-harmonic signal [Fig. 3(b)]. It has been observed in previous work that a single monolayer of a molecular adsorbate can greatly increase the SHG by a silver sample.[32] In this case, we associate the change in second-harmonic signal with the first adsorbed layer of AgCN on the silver substrate. The higher symmetry of the $[Ag(CN)_n]^{(n-1)-}$ complexes [59] suggests that upon adsorption they would make a smaller contribution to the second-order nonlinearity than would adsorbed AgCN. In fact, while the Raman signal of the complexes grows to a substantial strength at the conclusion of the reduction half-cycle, the second-harmonic signal falls markedly at the same time. Supposing that the SHG does indeed arise principally from a monolayer of AgCN adsorbed directly on the silver substrate, we then can understand the variation in the second-harmonic signal of Fig. 3(b)

in the following manner. The initial rise in the signal results from the oxidation of Ag to AgCN. Such a gradual rise in the surface coverage of AgCN has actually been predicted in a model of the electropolishing of silver.[60] After point a has been passed, the SHG decreases. This fall is expected as silver begins to be oxidized to Ag_2SO_4 (Ref. 56) [or possibly to Ag_2O (refs. 59,60)], causing the layer of AgCN to be removed from direct contact with the silver surface. The remarkable feature of the second-harmonic signal is the dramatic increase seen at the beginning of the reduction half-cycle. We interpret this jump as the consequence of reformation of AgCN at the silver surface as the interposed Ag_2SO_4 (or Ag_2O) layer is reduced. The second-harmonic output then remains large until the AgCN is fully reduced at the end of the cycle.

We have also performed a set of analogous measurements with a KCℓ (0.1M) electrolyte. The principal difference in the behavior with the KCℓ and K_2SO_4 electrolytes stems from the low solubility of AgCℓ compared with that of the Ag_2SO_4 salt. The low solubility of AgCℓ leads to the formation of a thick layer of this salt on the silver electrode during the oxidation half-reaction. Essentially all of the charge is then recovered as this deposit is reduced to pure silver. For the case of the pure KCℓ electrolyte, the voltammogram obtained by ramping the Ag-Pt bias at a constant rate from -2.0V to +2.5V and back to -2.0V in 4 minutes is displayed in Fig. 4(a). The second-harmonic signal [Fig. 4(b)] assumes a relatively constant value after the oxidation of just a few monolayers of silver, dropping sharply only at the end of the reduction half-cycle. As we have discussed above (and also in Ref. 32), this type of profile for the second-harmonic signal can be explained by the fact that symmetry considerations imply

that only the layer of AgCℓ in immediate contact with the silver electrode should contribute effectively to the SHG process. The polar AgCℓ structure appears to have a significant second-order nonlinearity.

Fig. 5 shows the experimental results for the same cycling in a KCℓ electrolyte with 0.01M KCN added. The second-harmonic signal resembles that obtained in the absence of any KCN. The particularly pronounced rise in the SHG at the start of the oxidation half-reaction is attributed to the formation of AgCN. As AgCℓ also gives rise to appreciable SHG, the signal remains large while the silver surface is covered with AgCℓ or AgCN. The second-harmonic signal drops again with the full reduction of the adsorbed layers. The SERS output for the 2110 cm^{-1} Stokes shift of the C-N stretch in $[Ag(CN)_3]^{2-}$ exhibits a behavior complementary to that of the second-harmonic: it is appreciable only before any oxidation and after full reduction of the silver surface, at which times direct adsorption of the complexes on the bare metal surface should be possible.

Following the completion of an oxidation-reduction cycle, the SHG and $[Ag(CN)_3]^{2-}$ SERS (2110 cm^{-1}) were monitored as a function of the reverse bias voltage. The experimental dependences of these two signal are plotted against V_{Ag-SCE} in Fig. 6. Essentially no current flowed as the reverse bias was increased up to $|V_{Ag-SCE}| \sim 1.2V$, at which point electrolysis of water was observed. The relatively small change in Raman scattering indicates that the chemical nature of the surface is not greatly affected by the reverse bias. On the other hand, the abrupt increase in SHG then suggests a bias-induced reorientation of the adsorbed silver-cyanide complexes. Such a reorientation could lower the symmetry of the adsorbed complexes and increase their contribution to the second-order non-

linearity. In any case, a simple change in the surface coverage of the complexes cannot explain the variation with bias of both the SHG and SERS.

A different comparison of SHG and SERS also indicates the occurrence of an orientational reordering. Here we discuss briefly our measurements with the two optical probes of cyanide adsorbed on silver in air and in an aqueous environment. We prepared an electrolytically roughened silver sample by first soaking it for several minutes in distilled water and then in water with 0.1M KCN. The silver sample was subsequently withdrawn from solution and thoroughly rinsed with distilled water. By methods of radioactive tracers, it has been determined that such a procedure leads to a silver surface with CN radicals present at approximately monolayer coverage.[61] Just as in previous investigations,[13-15,59-63] we observed a strong Raman line at ~ 2150 cm^{-1} from the cyanide-treated surface. The exact identity of the adsorbed species has not yet been established firmly. Recent studies of Laufer et al.[63] suggest that it is either the $[Ag(CN)_2]^-$ or the $[Ag_2(CN)_3]^-$ complex. Whatever the nature of the cyanide adsorbate, the SERS signal (centered at ~ 2150 cm^{-1}) remained unchanged as the sample was again submerged in distilled water. In the case of SHG, the cyanide-treated and untreated samples gave the same signal in air; in distilled water, however, the cyanide-treated sample was 3 times stronger than that of the untreated sample. Given the similarity of the Raman scattering, it seems that the chemical nature of the adsorbates has not changed upon introduction of the sample into water. The change in the second-harmonic signal can then be understood as the result of a reorientation of the adsorbed silver-cyanide complexes in water. The aqueous environment may stabilize the adsorbates, causing them to align more nearly along the surface normal. Such

a reorientation should further reduce the inversion symmetry of the surface, thus enhancing the second-harmonic signal.

In summary, we have seen that both SERS and SHG can be correlated with the presence of various adsorbates on a silver surface, although the two probes may be sensitive to different species. The SHG process requires a lack of inversion symmetry and is, consequently, strongly influenced by molecular orientation and symmetry.

B. Surface Enhancement of Raman Scattering and SHG

As a test of our theory of local-field enhancements, we have determined experimentally the enhancements shown by Raman and second-harmonic signals from an electrochemically reformed silver surface. The Raman enhancement was found for the 1005 cm^{-1} vibrational mode of adsorbed pyridine. Pyridine was chosen as the adsorbate for the relative simplicity of its surface chemistry and for the ease in making reference measurements from the neat liquid. The enhancement of the second-harmonic radiation was that of the silver substrate itself. Both measurements were performed on the same sample under the same 0.683 μm excitation.

The silver electrode was prepared by several of the conventional electrochemical cyclings in a pure 0.1M KCℓ electrolyte prior to the addition of pyridine (0.05M) and a final cycling. The p-polarized pump beam fell on the silver sample in solution at a 45° angle. The Raman signal from the adsorbed pyridine as recorded for V_{Ag-SCE} between -0.4V and -0.7V. In this range of potentials, it is believed that approximately a monolayer of pyridine is adsorbed to the silver surface.[1] A comparison of the signal from the adsorbed species (assumed to have a surface density of 4×10^{14}

cm^{-2}) can be made with that from an equal number of molecules in solution. This was accomplished by measuring the Raman scattering from neat pyridine with the same apparatus. After carefully accounting for the collection volume, we found the surface enhancement to be $\eta_R \sim 1.4 \times 10^6$. The surface-enhanced second-harmonic signal was also measured under the same conditions. Because of the large instrinsic nonlinearity of silver at 0.683 μm, the adsorbed pyridine did not materially change the SHG. The surface enhancement for SHG was determined by comparing the integrated strength of the angularly diffused signal from the roughened surface with that of the highly collimated harmonic output from a smooth, freshly evaporated silver film in pure water. The observed enhancement was $\eta_{SH} \sim 1 \times 10^2$; an enhancement of $\sim 1 \times 10^4$ was found for 1.06 μm excitation. In the latter case, no pyridine was introduced into the electrochemical cell in order to avoid any possible increase in SHG associated with this adsorbate.

We shall now see how well these experimental results for the Raman and second-harmonic enhancements can be explained by our theory of macroscopic local fields. From electron micrographs, the roughened silver surface is known to feature separated protrusions tens of nanometers in size. We model this topography by a perfectly conducting plane covered randomly with metal hemispheroids of varying dimensions. Interactions between the different protrusions are neglected, so the formulas of our previous analysis can be applied immediately. Since the spheroids have various aspect ratios, some of them should be appropriately shaped to exhibit a localized surface plasmon resonance and the accompanying large local-field enhancement at the frequency of the pump laser. Scattering from these structures should

be dominant. (Structures resonant at the harmonic frequency for SHG should make a much smaller contribution; those resonant at the Stokes-shifted frequency for Raman scattering should give a comparable contribution, which will be neglected.) The dimensions of the resonant protrusions can be determined in the following manner. According to Eq. (17), the criterion for resonance is $\mathrm{Re}[\varepsilon + (\varepsilon_m - \varepsilon)A] = 0$. For our case, $\varepsilon_m(\omega) = -22 + i0.4$, $\varepsilon_m(2\omega) = -1.3 + i0.3$ (Ref. 64), and $\varepsilon = \varepsilon_{water} = 1.77$, whence a resonance occurs at ω for $A = 0.074$. This value of the depolarization factor corresponds to a hemispheroid with aspect ratio $a/b = 4.1$ (Ref. 45). In the simple theory of Sec. II, the overall scale of the resonant structures does not affect the local-field enhancement. In reality, radiation damping limits the enhancement for large structures, and surface scattering increases the imaginary part of the dielectric constant for small structures, again limiting the enhancement. According to the work of Wokaun et al.,[15] the optimal enhancement for excitation of wavelength λ occurs for spheroids of volume $V \sim 10^{-4}\lambda^3$. With an effective radiating volume of $V = \frac{4\pi}{3} ab^2$, we then infer a semimajor axis $a \sim 50$ nm and a semiminor axis $b \sim 12$ nm.

For a hemispheroid of the specified dimensions, we can evaluate the macroscopic local-field factors of Eq. (17). Setting $\varepsilon' = \varepsilon$ here and below and including radiation damping and small size effects as in Ref. (15), we obtain $L_\perp(\omega) = 120$, $L_\parallel(\omega) = 9$, and $L_\parallel(2\omega) = 1.0$. In order to estimate η_{SH}, we must also evaluate the local-field correction factors for the flat silver surface. From Eq. (7), we find with the specified dielectric constants, $L_\perp(\omega) = 1.9$, $L_\parallel^p(\omega) = 0.7$, and $L_\parallel^p(2\omega) = 1.7$. The surface enhancement is now given directly by Eq. (21) as $\eta_{SH} = 1.0 \times 10^5$, which ex-

ceeds the experimental value by a factor of 1000. We must consider, however, that on our electrolytically roughened silver surface, the protrusions of tens of nanometers in size are separated from one another by hundreds of nanometers and that only a fraction of these structures will be in resonance. Hence, the theoretically predicted enhancement should be reduced by the fractional surface area f of the structures resonant at the laser frequency. In order to make theory agree with experiment, f should be 0.10%, which seems reasonable.

In the case of Raman scattering, we shall apply the theory in which only the $\perp\perp$-component of the Raman polarizability is important. This approximation is justified since $L_\perp(\omega)/L_\parallel(\omega) \sim 10$ at the laser frequency. The anticipated Raman enhancement, according to Eq. (19), is then $\eta_R = 6 \times 10^6$. The local-field correction factors entering this calculation are $L_\perp(\omega) = 120$ and $L_\perp(\omega_s) = 75$; the broadness of the strong resonant enhancement can be attributed to the radiation damping and small size effects. Taking the value of f deduced above, we predict an average enhancement of $f\eta_R = 6 \times 10^3$. This is~200 times less than the observed enhancement. The discrepancy can be understood as an additional enhancement arising from microscopic local-field effects and chemical interactions of the adsorbed pyridine with the silver surface, which have not been included in our theory. The enhancement not treated by our theory is essentially that exhibited by Raman scattering of adsorbates on a planar surface, in which case the macroscopic local-field corrections are comparatively minor. Udagawa et al.[9] have recently made measurements of the surface enhancement in ultrahigh vacuum for the same 1005 cm^{-1} mode of pyridine adsorbed on a (100) face of crystalline silver which was considered smooth. They report

a value of $\lesssim 440$ for the enhancement with excitation at 0.514 μm.

Consider now the surface enhancement for excitation at 1.06 μm. The relevant dielectric constants[64] are $\varepsilon_m(\omega) = -58 + i0.6$ and $\varepsilon_m(2\omega) = -12 + i0.4$. The local surface plasmon resonance at ω occurs for A = 0.030, i.e., for a structure with a/b = 7.7. Following the same procedure as above, we deduce a ~ 120 nm and b ~ 16 nm for those hemispheroids with maximal local-field correction factors of $L_\perp(\omega) = 190$, $L_\parallel(\omega) = 6$, and $L_\parallel(2\omega) = 1.4$. We observe that here the local-field factor $L_\perp$ assumes a larger value than was previously deduced for excitation at 0.683 μm. This behavior can be understood in terms of the lightning rod effect manifested by the very slender structures that are resonant at the longer wavelength. The local-field factors for the flat surface are $L_\perp(\omega) = 1.9$, $L_\parallel^p(\omega) = 0.5$, $L_\parallel^p(2\omega) = 0.8$, yielding $\eta_{SH} = 7 \times 10^5$. The predicted enhancement agrees with the experimental value of 1×10^4 for a fractional surface coverage of resonant structures of f~1.4%. [Because of the highly elongated shape of the resonant structures, f=1.4% corresponds to a coverage of just 0.11% for the projected (as opposed to the surface) area of the hemispheroids.] With this value for f, we can predict the average local-field enhancement of SERS. For a 1005 cm^{-1} Stokes shift, $L_\perp(\omega_s) = 120$ and Eq. (19) gives an average enhancement of $f\eta_R = 8 \times 10^4$ for a p-polarized pump incident at 45°. Microscopic local-field and chemical effects may further augment the signal. Using the same 200-fold increase deduced for the 0.683 μm excitation, we expect to observe a total enhancement of $\sim 2 \times 10^7$ in the Raman scattering of 1.06 μm light by pyridine adsorbed on our electrolytically reformed silver surface . To our knowledge, SERS has not been observed with a 1.06 μm pump laser. Our estimate, however, indicates that

the expected enhancement is actually somewhat larger than for excitation in the visible.

V. Concluding Remarks

In these experiments, we have seen how both SERS and SHG can be used to monitor molecular adsorption and desorption during an electrolytic cycle. While the two signals could be correlated with the surface chemistry, they were surprisingly different from one another. This dissimilarity appears to be the consequence of the more sensitive dependence of the second-harmonic signal on molecular symmetry and orientation.

Our treatment of the macroscopic local-field enhancement relied on a simple model of noninteracting hemispheroids on a conducting plane. Nonetheless, this model was capable of predicting the local-field correction factors, the surface enhancement, the dispersion of this enhancement, and the fractional coverage of resonant structures, all of which were fairly reasonable from the experimental point of view.

The general formalism of local-field enhancement presented in this paper should be applicable not only to local fields near a surface, metal or dielectric, but also to effects in the bulk. We shall not pursue this matter further, other than to give one additional example for a surface. Relying on our previously developed model for an electrochemically treated silver sample, we can calculate the emitted power for any surface optical process immediately. Here we consider the case of coherent anti-Stokes Raman scattering (CARS). We shall assume that only the $\alpha^{(3)}_{\perp\perp\perp\perp}$ term of the relevant third-order nonlinear polarizability for the adsorbed molecular layer is significant. The radiated power at the anti-Stokes frequency

$\omega_a = 2\omega - \omega_s$ from a highly elongated hemispherical boss is found in the manner of Sec. II to be

$$\mathcal{P}_{CARS}(\omega_a) = (2^{11}\pi^2 c\sqrt{\varepsilon}/3)(\omega_a/c)^4 (b/a)^8 N^2 a^4 \times$$

$$\times \left|\alpha^{(3)}_{\perp\perp\perp\perp} L_\perp(\omega_a) L_\perp(\omega_s) L^2_\perp(\omega)\right|^2_{spheroid} E^2(\omega_s) E^4(\omega) \sin^6\theta. \qquad (24)$$

It is assumed here that both pump beams (frequencies ω_s and ω) are p-polarized and incident on the base plane at angle θ. The local-field factors are those of Eq. (17) and all other symbols are as defined before. By way of comparison, the CARS output from an area $\mathcal{A}$ of a smooth surface is

$$\mathcal{P}_{CARS}(\omega_a) = (2\pi c/\sqrt{\varepsilon})(\omega_a/c)^2 N^2 \mathcal{A} \left|\alpha^{(3)}_{\perp\perp\perp\perp} L_\perp(\omega_a) L_\perp(\omega_s) L^2_\perp(\omega)\right|^2_{plane} \times$$

$$\times \sec\theta \sin^8\theta. \qquad (25)$$

Here the local-field factors are given by Eq. (7). Forming the ratio of these expressions, we then deduce the surface enhancement of the CARS process:

$$\eta_{CARS} = (2^{11}/3\pi)(b/a)^7 (k_a a)^2 \cos\theta \csc^2\theta \frac{\left|L_\perp(\omega_a) L_\perp(\omega_s) L^2_\perp(\omega)\right|^2_{spheroid}}{\left|L_\perp(\omega_a) L_\perp(\omega_s) L^2_\perp(\omega)\right|^2_{plane}}, \qquad (26)$$

with $k_a = \sqrt{\varepsilon}\, \omega_a/c$. For a rough surface with only a fractional surface area f occupied by structures with large enhancements, the predicted enhancement must be reduced proportionately.

Let us now make a numerical estimate of the surface enhancement of CARS in the case of a silver sample with pump excitation (ω) at 0.683 μm. For the optimally sized hemispheroid of a ~ 50 nm and b ~ 12 nm, $L_\perp(\omega) = 120$ and $L_\perp(\omega_a) \approx L_\perp(\omega_s) = 75$ for a 1005 cm^{-1} Stokes shift. Then taking $f = 0.10\%$ and $\theta = 45°$, as before, we deduce $f\eta_{CARS} = 3 \times 10^8$. Earlier we estimated that the microscopic local-field effects and the molecule-silver interaction enhanced the Raman cross-section σ_R of the 1005 cm^{-1} mode of pyridine by a further factor of ~ 200 Since $\alpha^{(3)} \propto \sigma_R$, the total surface enhancement for CARS should be on the order of $(200)^2 f\eta_{CARS} = 1.2 \times 10^{13}$. The absolute signal strength is predicted by Eq. (23) increased by the average enhancement of $(200)^2 f\eta_{CARS}$. For a 1 cm^2 silver surface covered by an adsorbate with a nonlinearity[65] $N\alpha^{(3)}_{\perp\perp\perp\perp} = 10^{-20}$ esu, we expect emission of 3×10^5 photons/pulse for pump excitation of 10 ns duration and a modest fluence of 1 mJ/cm^2. This anti-Stokes output should be readily observable if not overwhelmed by a background from the silver substrate. In this connection, it should be noted that although surface CARS is obviously a coherent process, the presence of the roughened surface needed for a macroscopic local-field enhancement may cause the anti-Stokes output to be angularly diffused and potentially difficult to distinguish from incoherently scattered light.

References

1. M. Fleischmann, P. J. Hendra, and A. J. McQuillan, Chem. Phys. Lett. 26, 163 (1974); D. L. Jeanmaire and R. P. van Duyne, J. Electroanal. Chem. 84, 1 (1977); M. G. Albrecht and J. A. Creighton, J. Am. Chem. Soc. 99, 5215 (1977).

2. For a recent review see Surface Enhanced Raman Scattering, edited by R. K. Chang and T. E. Furtak (Plenum, New York, 1982).

3. R. R. Smardzewski, R. J. Colton, and J. S. Murday, Chem. Phys. Lett. 68, 53 (1979).

4. P. N. Sanda, J. M. Warlaumont, J. E. Demuth, J. C. Tsang, K. Christmann, and J. A. Bradley, Phys. Rev. Lett. 45, 1519 (1980).

5. H. Seki and M. R. Philpott, J. Chem. Phys. 73, 5376 (1980).

6. T. H. Wood, D. A. Zwemer, C. V. Shank, and J. E. Rowe, Chem. Phys. Lett. 82, 5 (1981) and references therein.

7. J. C. Tsang, J. R. Kirtley, and T. N. Theis, Solid State Commun. 35, 667 (1980) and references therein.

8. C. A. Murray, D. L. Allara, and M. Rhinewine, Phys. Rev. Lett. 46, 57 (1981).

9. M. Udagawa, C.-C. Chou, J. C. Hemminger, and S. Ushioda, Phys. Rev. B 23, 6843 (1981).

10. D. A. Weitz, T. J. Gramila, A. Z. Genack, and J. I. Gersten, Phys. Rev. Lett. 45, 355 (1980).

11. A. Girlando, M. R. Philpott, D. Heitmann, J. D. Swalen, and R. Santo, J. Chem. Phys. 72, 5187 (1980).

12. C. Y. Chen, E. Burstein, and S. Lundquist, Solid State Commun. 32, 63 (1979); C. Y. Chen, I. Davoli, G. Ritchie, and E. Burstein, Surf. Sci.

101, 363 (1980).

13. J. G. Bergman, D. S. Chemla, P. F. Liao, A. M. Glass, A. Pinczuk, R. M. Hart, and D. H. Olson, Opt. Lett. 6, 33 (1981).

14. P. F. Liao, J. G. Bergman, D. S. Chemla, A. Wokaun, J. Melngailis, A. M. Hawryluk, and N. P. Economou, Chem. Phys. Lett. 82, 355 (1981).

15. A. Wokaun, J. P. Gordon, and P. F. Liao, Phys. Rev. Lett. 48, 957 (1982).

16. H. Wetzel and H. Gerischer, Chem. Phys. Lett. 76, 460 (1980).

17. K. U. von Raben, R. K. Chang, and B. L. Laube, Chem. Phys. Lett. 79, 465 (1981) and references therein.

18. T. E. Furtak and J. Kester, Phys. Rev. Lett. 45, 1652 (1980).

19. M. Moskovits, J. Chem. Phys. 69, 4159 (1978).

20. C. Y. Chen and E. Burstein, Phys. Rev. Lett. 45, 1287 (1980).

21. M. Kerker, D.-S. Wang, and H. Chew, Appl. Opt. 19, 4159 (1980); D.-S. Wang and M. Kerker, Phys. Rev. B 24, 1777 (1981).

22. S. L. McCall, P. M. Platzman, and P. A. Wolff, Phys. Lett. 77A, 381 (1980).

23. J. Gersten and A. Nitzan, J. Chem. Phys. 73, 3023 (1980); 75, 1139 (1981).

24. P. F. Liao and A. Wokaun, J. Chem. Phys. 76, 751 (1982).

25. B. J. Messinger, K. U. von Raben, R. K. Chang, and P. W. Barber, Phys. Rev. B 24, 649 (1981) and references therein.

26. D. V. Murphy, K. U. von Raben, R. K. Chang, and P. B. Dorain, Chem. Phys. Lett. 85, 43 (1982).

27. A. Harstein, J. R. Kirtley, and J. C. Tsang, Phys. Rev. Lett. 45, 201 (1980).

28. A. M. Glass, A. Wokaun, J. P. Heritage, J. G. Bergman, P. F. Liao, and D. H. Olson, Phys. Rev. B 24, 4906 (1981).

29. G. Ritchie and E. Burstein, Phys. Rev. B 24, 4843 (1981) and reference therein.

30. C. K. Chen, A. R. B. de Castro, and Y. R. Shen, Phys. Rev. Lett. 46, 145 (1981).

31. A. Wokaun, J. G. Bergman, J. P. Heritage, A. M. Glass, P. F. Liao, and D. H. Olson, Phys. Rev. B 24, 849 (1981).

32. C. K. Chen, T. F. Heinz, D. Ricard, and Y. R. Shen, Phys. Rev. Lett. 46, 1010 (1981).

33. T. F. Heinz, C. K. Chen, D. Ricard, and Y. R. Shen, Chem Phys. Lett. 83, 180 (1981).

34. G. R. Erdheim, R. L. Birke, and J. R. Lombardi, Chem. Phys. Lett. 69, 495 (1980).

35. R. Dornhaus, M. B. Long, R. E. Benner, and R. K. Chang, Surf. Sci. 93, 240 (1980).

36. C. J. F. Böttcher and P. Bordewijk, Theory of Electric Polarization, 2nd ed. (Elsevier, Amsterdam, 1978).

37. A. Bagchi, R. G. Barrera, and B. B. Dasgupta, Phys. Rev. Lett. 44, 1475 (1980).

38. F. W. King, R. P. van Duyne, and G. C. Schatz, J. Chem. Phys. 69, 4472 (1978); G. C. Schatz and R. P. van Duyne, Surf. Sci. 101, 425 (1980).

39. S. Efrima and H. Metiu, J. Chem. Phys. 70, 1602 (1979); 70, 2297 (1979); T. Maniv and H. Metiu, J. Chem. Phys. 72, 1996 (1980).

40. W. H. Weber and G. W. Ford, Phys. Rev. Lett. 44, 1774 (1980); G. W. Ford and W. H. Weber, Surf. Sci. 109, 451 (1981).

41. J. A. Armstrong, N. Bloembergen, J. Ducuing, and P. S. Pershan, Phys. Rev. 127, 1918 (1962).

42. While we have not established the general conditions for the validity of this expression, we have verified its correctness in each case considered in this paper by a full solution of Maxwell's equations for the incoming and outgoing fields.

43. Here we have adopted the convention that the real electric field is $\vec{E}(t) = \vec{E}(\omega)e^{-i\omega t} + \vec{E}^*(\omega)e^{+i\omega t}$.

44. J. A. Stratton, Electromagnetic Theory (McGraw-Hill, New York, 1941), Ch. 3.

45. Generally, $A = [1 - \xi Q_1'(\xi)/Q_1(\xi)]^{-1}$ with Legendre function of the second kind $Q_1(\xi) = (\xi/2)\ell n[(\xi + 1)/(\xi - 1)] - 1$ and $\xi = [1 - (b/a)^2]^{-\frac{1}{2}}$. For this formula and explicit tabulations of A, see J. A. Osborn, Phys. Rev. 67, 351 (1945) and E. C. Stoner, Philos. Mag. 36, 803 (1945). We can rewrite $L_{\|} = (\varepsilon'/\varepsilon_m)L_{\perp} = [Q_1(\xi) - \xi Q_1'(\xi)]/[(\varepsilon_m/\varepsilon)Q_1(\xi) - \xi Q_1'(\xi)]$.

46. N. Bloembergen, R. K. Chang, S. S. Jha, and C. H. Lee, Phys. Rev. 174, 813 (1968); 178, 1528(E) (1969).

47. J. Rudnick and E. A. Stern, Phys. Rev. B 4, 4274 (1971) and references therein.

48. C. S. Wang, J. M. Chen, and J. R. Bower, Opt. Commun. 8, 275 (1973).

49. J. R. Bower, Phys. Rev. B 14, 2427 (1976).

50. J. E. Sipe, V. C. Y. So, M. Fukui, and G. I. Stegeman, Phys. Rev. B 21, 4389 (1980).

51. This statement is valid for excitation of a flat surface by a single plane wave. It also holds generally for any excitation of an arbitrarily shaped surface provided that only the $\|\perp\|$-component of $\overleftrightarrow{\chi}_s$ is non-

zero. See C. C. Wang, Phys. Rev. 178, 1475 (1969).

52. H. Sonnenberg and H. Heffner, J. Opt. Soc. Am. 58, 209 (1968).

53. C. C. Wang and A. N. Duminski, Phys. Rev. Lett. 20, 668 (1968); 21 266(E) (1968).

54. For a calculation of SHG by a small metal sphere with a free electron response, see G. S. Agarwal and S. S. Jha, Solid State Commun. 41, 499 (1982).

55. We shall use the same approximation in the case of 1.06 μm excitation, for which the given term and the bulk polarization are believed to contribute approximately equally to SHG from a planar silver surface under p-polarized excitation. In our discussion, we shall neglect any possible variation in the coefficient β as a function of the surface structure on an atomic scale. Both of these points are treated in Ref. 47.

56. R. E. Benner, R. Dornhaus, R. K. Chang, and B. L. Laube, Surf. Sci. 101, 341 (1980).

57. T. E. Furtak, G. Trott, and B. H. Loo, Surf. Sci. 101, 374 (1980); T. E. Furtak, Solid State Commun. 28, 903 (1978).

58. J. Timper, J. Billmann, A. Otto, and I. Pockrand, Surf. Sci. 101, 348 (1980) and references therein.

59. J. Billmann, G. Kovacs, and A. Otto, Surf. Sci. 92, 153 (1980).

60. A. N. Lebedev, V. V. Gubailovskii, and I. A. Kakovskii, Zhurnal Prikladnoi Khimii 49, 577 (1976). [*English translation:* J. Appl. Chem. USSR 49, 589 (1976)]

61. J. G. Bergman, J. P. Heritage, A. Pinczuk, J. M. Worlock, and J. H. McFee, Chem. Phys. Lett. 68, 412 (1979).

62. J. P. Heritage, J. G. Bergman, A. Pinczuk, and J. M. Worlock, Chem. Phys. Lett. 67, 229 (1979).

63. G. Laufer, J. T. Huneke, and T. F. Schaaf, Chem. Phys. Lett. 82, 571 (1981).

64. P. B. Johnson and R. W. Christy, Phys. Rev. B 6, 4370 (1972).

65. P. D. Maker and R. W. Terhune, Phys. Rev. 137, A801 (1965).

(a) Permanent address: C-232, Lincoln Laboratories, 244 Wood St., Lexington, MA 02173.

(b) On leave from Ecole Polytechnique, Laboratoire d'Optique Quantique, Route de Saclay, 91128 Palaiseau, France.

(c) Miller professor at the University of California, Berkeley.

Figure Captions

Fig. 1. Schematic representation of the experimental set-up for SERS and SHG measurements of electrochemical processes on a silver electrode.

Fig. 2. Data for an oxidation-reduction cycle of the silver electrode in a 0.1M K_2SO_4 electrolyte. The voltammogram is shown in (a); electrode voltage V_{Ag-SCE}, electrolytic current I, and second-harmonic signal are presented as functions of time in (b).

Fig. 3. Same as in Fig. 2, but with 0.01M KCN added to the electrolyte. The SERS measurement of (b) for the strength of the 2110 cm^{-1} line has been constructed after the results of Benner et al. [56]

Fig. 4. Data for an oxidation-reduction cycle of the silver electrode in a 0.1M KCℓ electrolyte.

Fig. 5. Same as in Fig. 4,but with 0.01M KCN added to the electrolyte. The SERS measurement was taken for a 2110 cm^{-1} Stokes shift.

Fig. 6. SHG and SERS (2110 cm^{-1}) from the silver electrode following the completion of an oxidation-reduction cycle as the applied bias is varied. Irreversible desorption occurred for $|V_{Ag-SCE}| > 1.2V$.

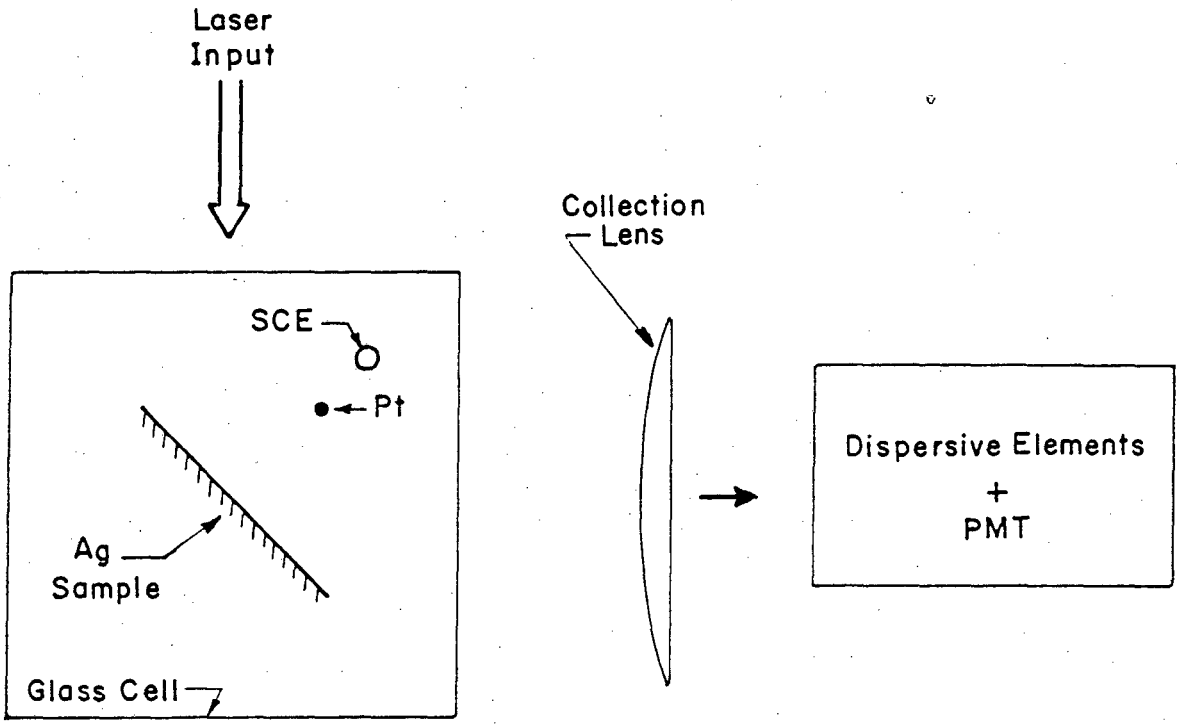
Laser
Input
SCE
Pt
Ag
Sample
Glass Cell
Collection
Lens
Dispersive Elements
+
PMT

XBL 824-5583

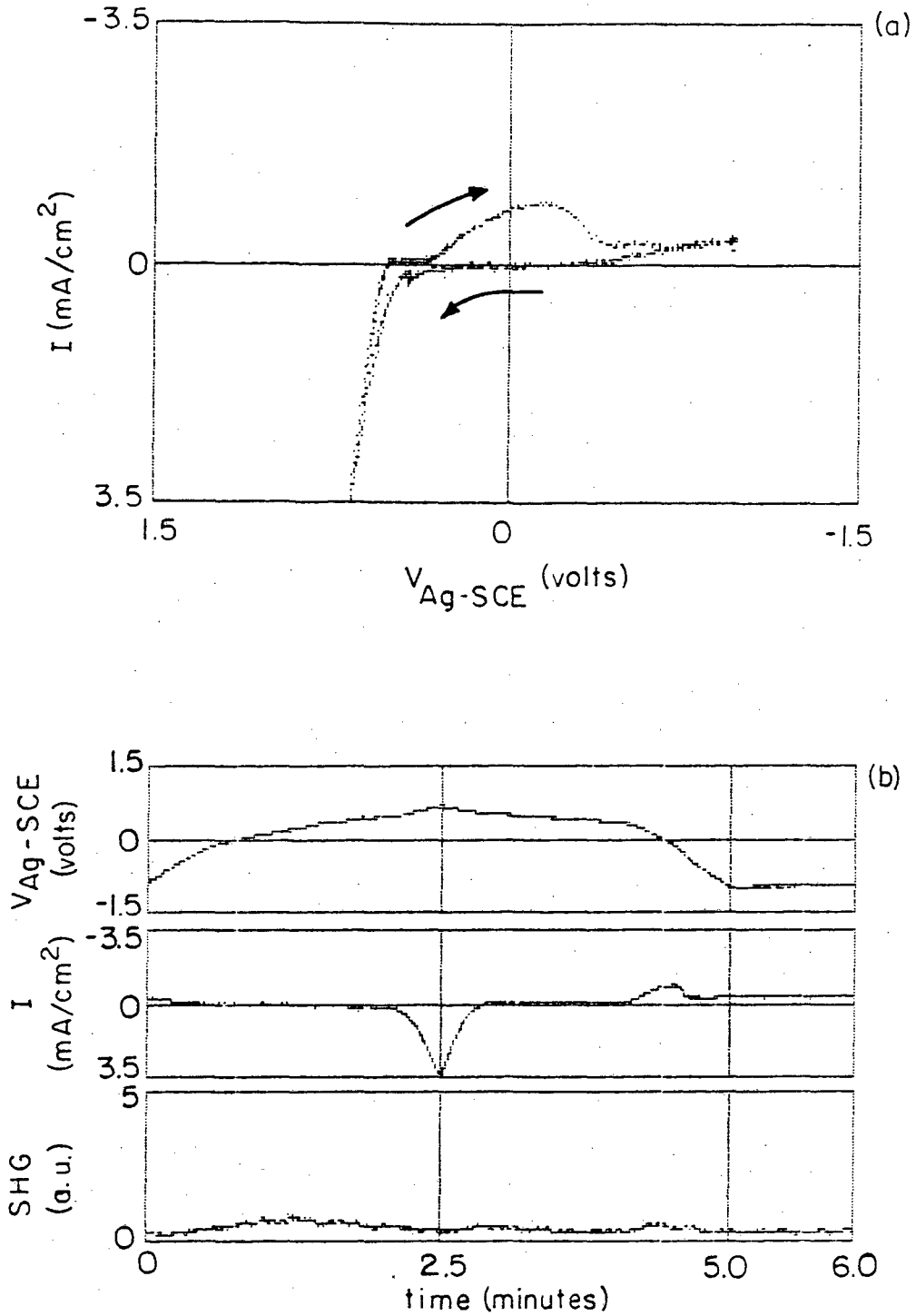
-3.5
0
3.5
I (mA/cm^2)
(a)
1.5
0
-1.5
V_{Ag-SCE} (volts)
1.5
0
-1.5
V_{Ag-SCE} (volts)
(b)
-3.5
0
3.5
I (mA/cm^2)
5
0
SHG (a.u.)
0
2.5
5.0
6.0
time (minutes)

XBL 824-5584

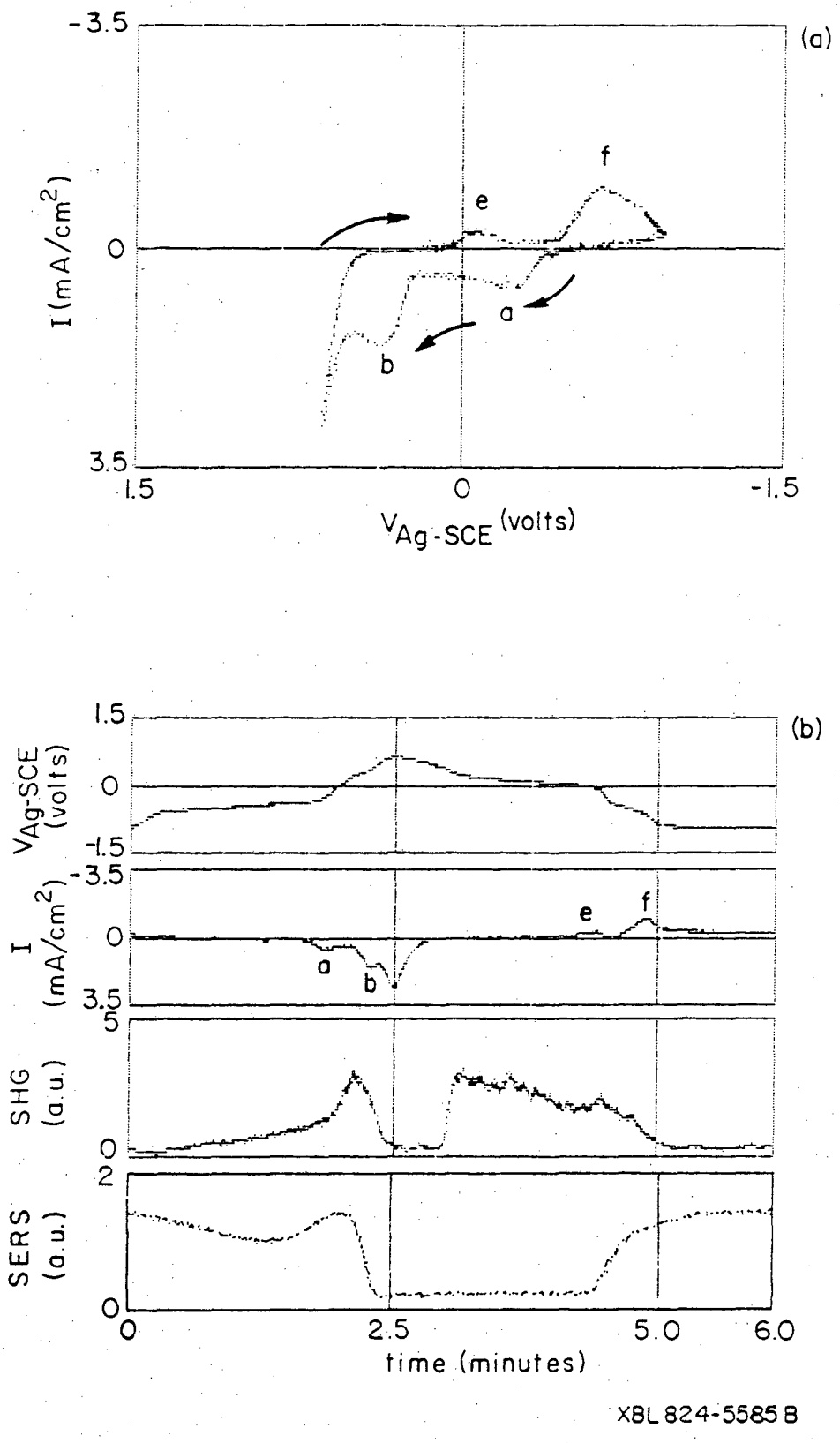
(a)
-3.5
0
3.5
I (mA/cm²)
f
e
a
b
1.5
0
-1.5
V Ag-SCE (volts)
(b)
1.5
0
-1.5
V Ag-SCE (volts)
-3.5
0
3.5
I (mA/cm²)
e
f
a
b
5
0
SHG (a.u.)
2
0
SERS (a.u.)
0
2.5
5.0
6.0
time (minutes)
XBL 824-5585 B

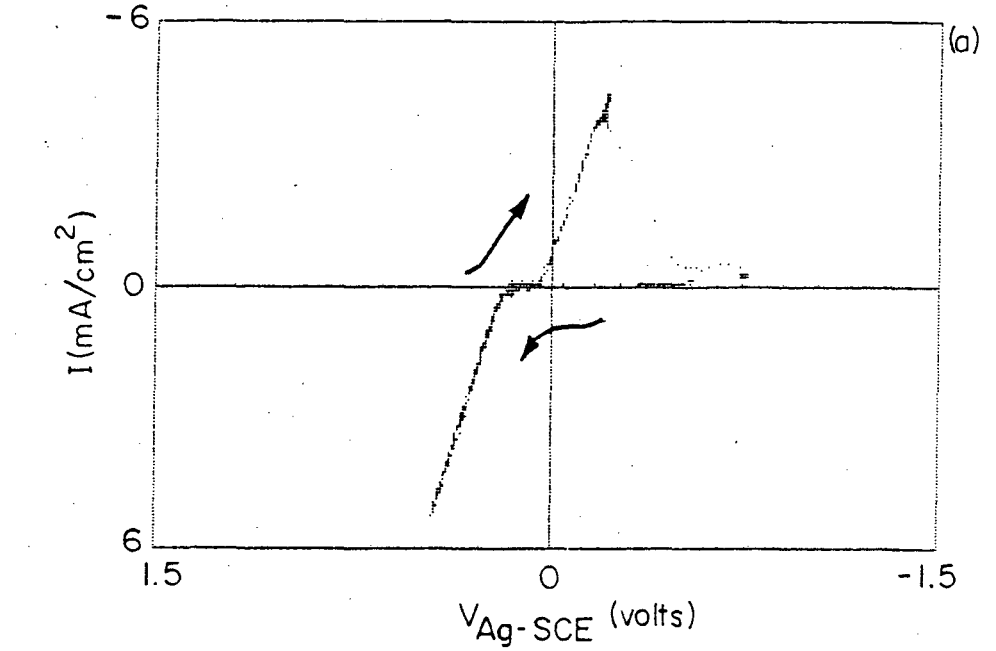
-6
0
6
I(mA/cm²)
(a)
1.5
0
-1.5
V Ag-SCE (volts)

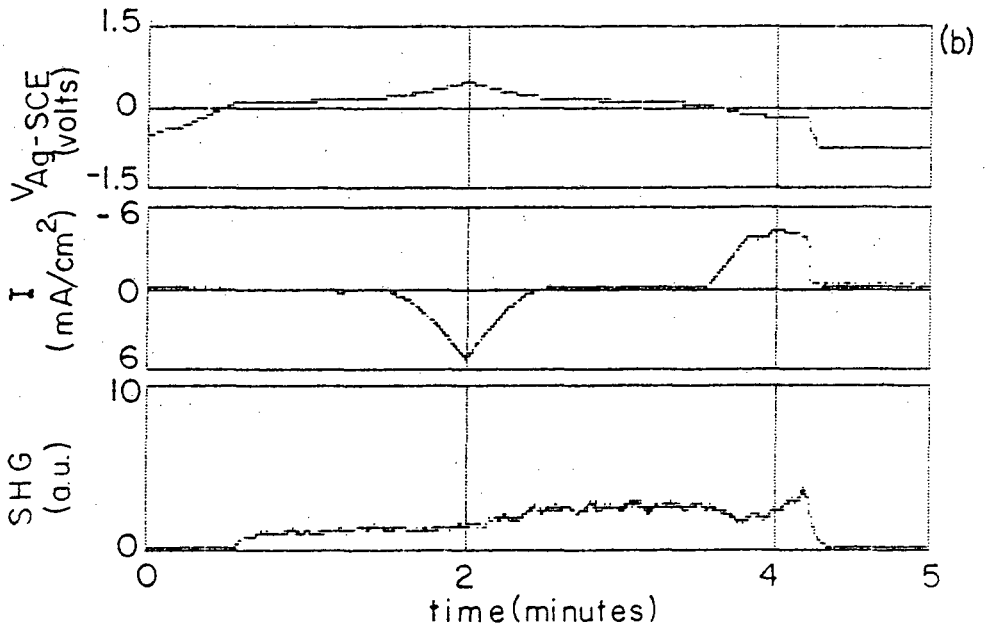
1.5
0
-1.5
V Ag-SCE (volts)
(b)
-6
0
6
I (mA/cm²)
10
0
SHG (a.u.)
0
2
4
5
time (minutes)

XBL 824-5586

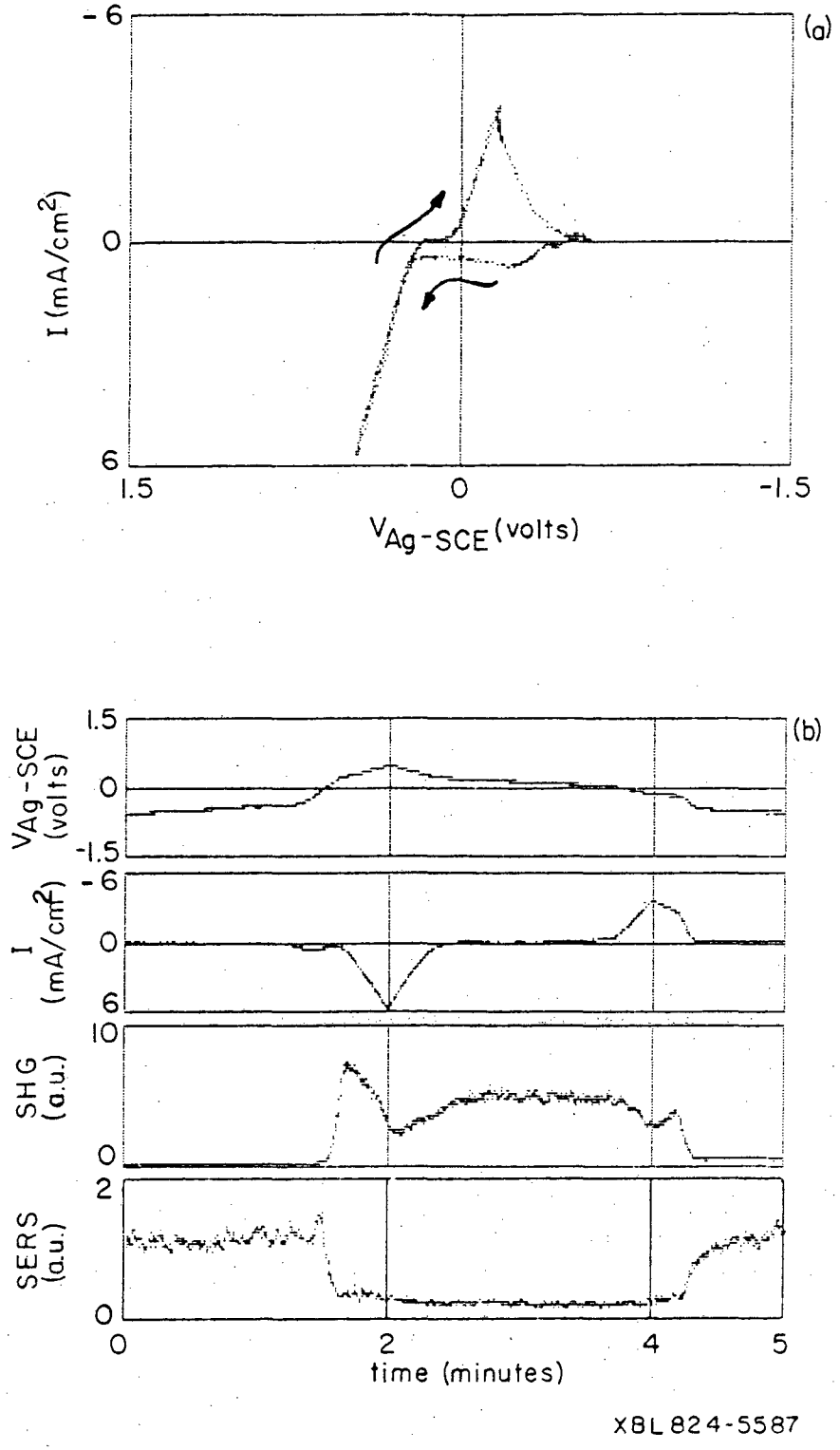
(a)
-6
0
6
I (mA/cm²)
1.5
0
-1.5
V Ag-SCE (volts)
(b)
1.5
0
-1.5
V Ag-SCE (volts)
-6
0
6
I (mA/cm²)
10
0
SHG (a.u.)
2
0
SERS (a.u.)
0
2
4
5
time (minutes)
XBL824-5587

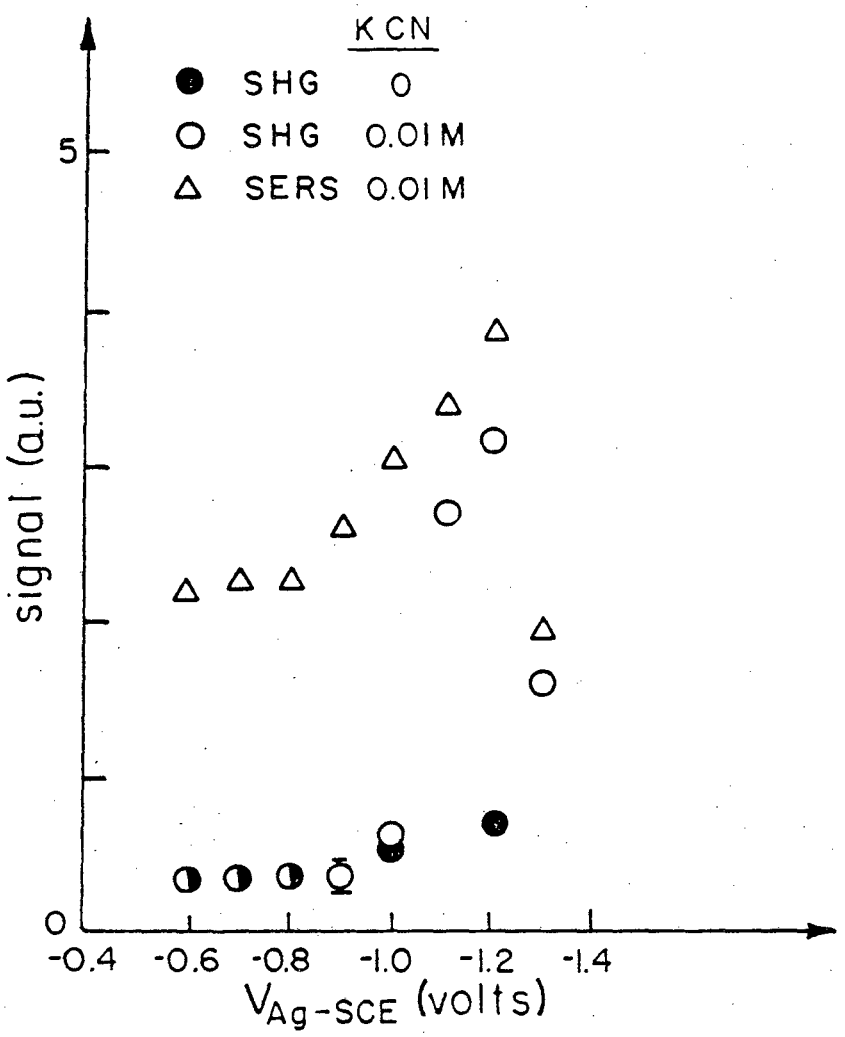
KCN
SHG 0
SHG 0.01 M
SERS 0.01 M
5
0
signal (a.u.)
-0.4
-0.6
-0.8
-1.0
-1.2
-1.4
V_{Ag-SCE} (volts)

XBL 824-5588

TECHNICAL INFORMATION DEPARTMENT
LAWRENCE BERKELEY LABORATORY
UNIVERSITY OF CALIFORNIA
BERKELEY, CALIFORNIA 94720